Cumhuriyet Sci. J., 46(4) (2025) 937-948
DOI: https://doi.org/10.17776/csj.1662124

Cumhuriyet Science Journal

| csj.cumhuriyet.edu.tr | Founded: 2002 ISSN: 2587-2680 e-ISSN: 2587-246X Publisher: Sivas Cumhuriyet University

Regression and Correlation-Based Modeling of Nonlinear Optical Response in Quantum Wells

Muhammed Sayraç[1,2, a,*], Emre Yalçın[3,b]

[1]*Institute of Science, Department of Artificial Intelligence and Data Science, Sivas Cumhuriyet University, Sivas, Türkiye*

[2]*Department of Nanotechnology Engineering, Sivas Cumhuriyet University, Sivas, Türkiye*

[3]*Computer Engineering Department, Sivas Cumhuriyet University, Sivas, Türkiye*

**Corresponding author*

Research Article

History
Received: 20/03/2025
Accepted: 06/10/2025

ABSTRACT

This study investigates the nonlinear optical properties of quantum wells (QWs) by analyzing the energy eigenvalues and eigenfunctions of confined electrons. The nonlinear optical rectification (NOR) coefficient was numerically calculated under various structural parameters and external fields. To establish relationships between the system's energy eigenvalues, dipole moment matrix elements, and NOR coefficient, regression and correlation analyses were conducted using IBM SPSS Statistics. Linear, quadratic, and cubic regression models were evaluated, with the cubic model demonstrating the best fit. Model accuracy was assessed using several evaluation metrics, including coefficient of determination (R^2), mean absolute percentage error (*MAPE*), mean absolute error (*MAE*), mean square error (*MSE*), and root mean square error (*RMSE*) values for different external factors (temperature, pressure, electric field, barrier width, and barrier thickness). The results indicate that predictive modeling of the NOR coefficient enhances experimental efficiency by reducing cost and time while providing a reliable framework for understanding the optical behavior of QWs. This study offers a data-driven approach to optimizing nonlinear optical responses, contributing to advancements in optoelectronic applications.

Keywords: Quantum wells, Nonlinear optical rectification, Regression analysis, Predictive modeling, Optoelectronics.

[a] *muhammedsayrac@cumhuriyet.edu.tr* *https://orcid.org/0000-0003-4373-6897* [b] *eyalcin@cumhuriyet.edu.tr* *https://orcid.org/0000-0003-3818-6712*

Introduction

In recent years, research on Nonlinear Optical materials (NLO) has increased rapidly. These materials have significant potential for use in various advanced technology fields, such as optoelectronics, photonics, and laser technologies [1]. NLO materials play a crucial role in applications such as optical signal modulation, signal processing, frequency conversion, optical memory, and ultrashort laser pulses. Understanding NLO responses is particularly related to processes such as nonlinear optical rectification (NOR), second-harmonic generation (SHG), and third-harmonic generation (THG). Therefore, advancements in materials science, nanotechnology, and manufacturing techniques have provided significant progress in controlling and optimizing NLO properties [2].

NLO materials are essential for directing, modulating, and amplifying optical signals. Research in this field focuses on developing materials with high nonlinear coefficients and low optical losses. Additionally, advancements in ultrafast laser technologies have provided new opportunities for studying NLO processes and have significantly contributed to investigating the time-resolved optical properties of these materials [1, 3, 4]. NLO optical responses, particularly NOR, SHG, and THG coefficients, have broad application potentials, such as infrared laser amplifiers, photodetectors, optical switches, and high-speed optical modulators [5, 6]. Due to their extensive technological applications, quantum nanostructures such as quantum wells, quantum dots, and quantum wires have become a focal point of interest in this field. Carrier confinement in these structures at limited dimensions leads to electron energy-level separations. The geometric parameters of the potential well (such as barrier height, barrier thickness, and well width) and external influences (such as electric, magnetic, and laser fields) cause significant changes in the optical and electronic properties of these structures [7, 8]. Precisely, the shape of the Quantum Well (QW) potential leads to shifts in the resonance peak values of nonlinear effects such as NOR, SHG, and THG across different energy regions [9, 10].

The separation of energy levels in quantum wells can be controlled by modifying the structure's geometric parameters (such as potential barrier height, barrier thickness, and well depth) [11, 12] and by applying external fields [13]. Changes in these parameters alter the shape of the QW potential, leading to significant variations in both linear and nonlinear optical properties [5, 14].

Experimental investigation of the behavior of QW structures under different structural parameters and external influences requires substantial time and financial resources. Considering the complexity of such experimental studies and issues of precision and reproducibility, exploring alternative methods for predicting QW behavior has become highly significant. In this regard, prediction-based modeling

approaches offer a potential solution by reducing the experimental requirements and costs associated with these structures. Such techniques enable the simulation and prediction of QW behavior under different parameters, providing faster and more cost-effective results than traditional methods. Studies in literature increasingly focus on characterizing QW structures and analyzing their behavior under various conditions using prediction-based methods [15, 16]. These studies highlight the potential of predictive analysis techniques for efficiently evaluating the performance of QW structures.

In this study, prediction-based regression and correlation analyses will be conducted to enable cost-effective and time-efficient predictions with high reproducibility. The effects of different external factors on the NOR coefficient will be analyzed using predictive modeling approaches, providing insights into the underlying mechanisms governing the optical properties of QW structures. The novelty of this study lies in leveraging predictive models to understand the impact of external fields on quantum wells. The relationship between external factors and NOR peak positions will be comprehensively explained through correlation and regression analyses.

Four research questions (RQs) have been formulated for this study. The findings will provide insights into how external fields influence NOR values and how the position of the maximum NOR peak shifts, either towards lower energy regions ("red shift") or higher energy regions ("blue shift").

RQ1. How do external factors (T, P, F, L_b, L_w) affect the relationship between energy values and dipole moment matrix elements in a quantum well?

RQ2. What is the correlation between the external fields and the maximum NOR values?

RQ3. How do different external fields influence the photon energy at the NOR peak, and what is its correlation with maximum NOR values?

RQ4. How do regression models describe the relationship between each parameter and the NOR coefficient, and what evaluation metrics are obtained?

Based on these analyses, the study aims to examine the behavior of QW structures under external influences using correlation and regression techniques, thereby determining the behavior of the NOR coefficient. To achieve this, a QW's energy values and eigenfunctions will be determined. Subsequently, dipole moment matrix elements will be extracted from these data. These values will then be analyzed using predictive models to investigate how different external fields influence the NOR coefficient.

External fields applied to the structure modify the energy levels of electrons in QW structures, affecting the NOR coefficient. Regression and correlation analyses will be used to model these interactions, providing a deeper understanding of the mechanisms underlying the optical properties of QW structures.

These investigations will contribute to understanding the influence of the NOR coefficient on the optical properties of QW structures, facilitating the development of more precise designs for future optoelectronic applications. Predictive models will enable a more in-depth analysis of the optical behavior of these structures, helping to identify which factors influence the NOR coefficient of QW structures. By integrating correlation and regression analyses with predictive modeling techniques, this study aims to comprehensively explain the relationship between external factors affecting QWs and NOR peak positions. Understanding the effects of various primary and secondary parameters on QW structures and predicting the NOR coefficient will be a crucial tool for designing more efficient, cost-effective, and precise future optoelectronic applications. These analyses hold potential for a broad range of applications, from materials science to optoelectronics, and are likely to form the foundation for future advancements in nonlinear optics.

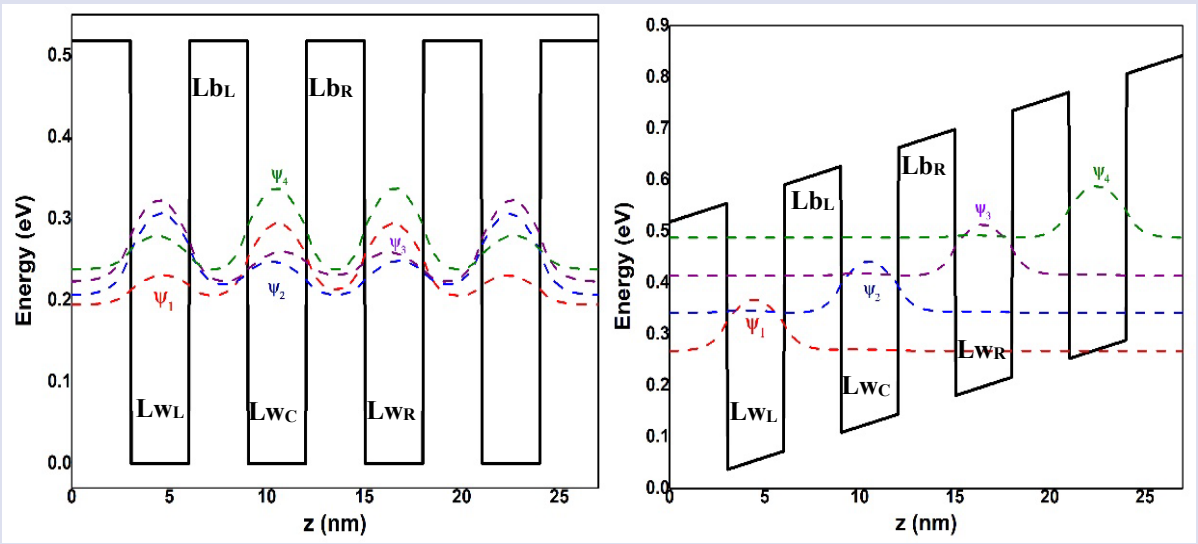

Figure 1. Quantum well structure with the first four energy wavefunctions. The structure parameters are set as Lb_L = Lb_R = 3 nm and Lw_L = Lw_C = 3 nm. The wavefunctions are shown under two different electric field conditions (a) F = 0 kV/cm (b) F = 90 kV/cm.

In Figure 1, the QW structure is presented. Lb_L and Lb_R represent the left and right barrier thicknesses, while Lw_L, Lw_C, and Lw_R denote the left and right well widths, respectively. The wavefunctions ψ_1, ψ_2, ψ_3, and ψ_4 correspond to the squared wavefunctions of electrons at the ground state, first, second, and third excited energy levels. The applied electric field (*F*), temperature (*T*), and pressure (*P*) on the QW can also alter the energy levels of the electrons. The effects of the five primary parameters (Lw_L, Lw_R, *F*, *T*, and *P*) that govern the energy levels of electrons in the well are examined in detail.

The effects of the five primary parameters applied to the quantum well structure depicted in Figure 1 lead to variations in the Nonlinear Optical Rectification (NOR) coefficient. Changes in the QW structure, such as variations in barrier thickness or the application of external fields like temperature, cause electrons to occupy different energy levels within the well. This phenomenon is based on quantum mechanical principles. Electrons in QW structures are confined to specific energy levels, and structural modifications or external influences can alter these levels. Consequently, this affects the movement of electrons within the well and their optical behavior. Understanding this process provides insight into how the optical properties of QW structures can be modified. The energy values and the dipole moment matrix element are calculated using quantum mechanical methods, considering the electron's state within the well. Before conducting experimental studies, the relationships between these primary and secondary parameters will be analyzed using regression and correlation methods to identify the connection between electron behavior and potential nonlinear optical properties.

Theory

In a quantum well structure, the confined electron's energy eigenvalues (E_{ij}) and energy eigenfunctions (ψ_i) are obtained by solving the Schrödinger wave equation. The Hamiltonian for a confined electron within the QW is given in Equation 1 [8, 10].

$$H = \frac{p_e^2}{2m^*(P,T)} + V(z,P,T) - eFz \tag{1}$$

In Equation 1, $m^*(P,T)$ represents the effective mass, p_e denotes the electron's momentum, *F* is the magnitude of the external electric field, and the z-axis indicates the direction of structural confinement. By solving Equation 1, the system's energy levels and corresponding wavefunctions can be determined. Consequently, the system's optical properties, particularly the nonlinear optical rectification (NOR) coefficient, can be controlled. The relationship between the applied pressure and temperature and the system's effective mass is expressed in Equation 2.

$$m^*(P,T) = m_0\left[1 + E_g^{\Gamma}\left(\frac{2}{E_g^{\Gamma}(P,T)} + \frac{1}{E_g^{\Gamma}(P,T)+0.341}\right)\right]^{-1} \tag{2}$$

Here, m_0 is the free electron mass [17], and E_g^{Γ} represents the energy band gap.

The sub-band energy levels and wavefunctions of electrons in a QW structure are obtained by solving the time-independent Schrödinger equation. The wavefunction describes the spatial distribution and behavior of electrons within the QW.

In the barrier regions surrounding the QW, the wave function decays exponentially as the electron moves away from the well. This indicates a very low probability of finding the electron outside the well. The exact form of the wavefunctions is influenced by various factors such as the thickness of the quantum well, the width of the barriers, and the applied external fields.

By solving the Schrödinger equation, energy values and corresponding wavefunctions are obtained after defining structural parameters dependent on hydrostatic pressure and temperature [6, 8].

The NOR coefficient is defined in Equation 3 [11]

$$\chi_0^{(2)} = \frac{4e^3\rho_{01}\delta_{01}\mu_{01}^2}{\varepsilon_0\hbar^2}\frac{\left[\omega_{01}^2\left(1+{\Gamma_2}/{\Gamma_1}\right)+(\omega^2+\Gamma_2^2)\left({\Gamma_2}/{\Gamma_1}-1\right)\right]}{\left[(\omega_{01}-\omega)^2+\Gamma_2^2\right]\left[(\omega_{01}+\omega)^2+\Gamma_2^2\right]} \tag{3}$$

here, ρ_{0i} represents the three-dimensional electron density ($\rho_{0i} = \rho_0 - \rho_i, i = 1,3$). The parameter $\mu_{ij} = \langle\psi_i|z|\psi_j\rangle, (i,j = 0,1,2,3)$ denotes diagonal matrix elements, which describe the interaction strength between two energy levels involved in electronic transitions. Additionally, δ_{01} is given by $\delta_{01} = |\mu_{00} - \mu_{11}|$, while $\omega_{ij} = {(E_i - E_j)}/{\hbar}$ represents the electron transition frequency. Finally, $\Gamma_k = {1}/{T_k}$ with k=1,2,3 is the relaxation rate coefficient related to the electron transition lifetime. The constants used to compute the NOR coefficient can be defined as follows. $m^* = 0.067m_0$ (where m_0 is the free electron mass), electron charge $e = 1.602 \times 10^{-19}C$, $\hbar = 1.056 \times 10^{-34}Js$, $\rho_{01} = \rho_{01} = 3 \times 10^{22}m^{-3}$, $\mu = 4\pi \times 10^{-7}Hm^{-1}$, $\varepsilon_0 = 8.854 \times 10^{-12}$, and $\Gamma_k = 1,3,5\ THz$ (k = 1,2,3).

Once the system's energy eigenvalues and eigenfunctions are obtained, the variation of the NOR coefficient will be examined using regression and correlation analysis to determine its dependency on external factors.

After calculating the system's energy eigenvalues and the corresponding eigenfunctions, the results will be used to analyze the behavior of the structure's NOR coefficient. During this analysis, regression and correlation techniques will be employed to examine the dependence of the NOR coefficient on external fields. The accuracy and significance of the results will be statistically tested. Thus, a better understanding of physical variables' effects on the system's NOR coefficient will be achieved. Additionally, three models will be applied: linear regression, cubic regression, and quadratic regression. After the regression analysis, evaluation metrics will be obtained, namely the R^2 value, mean absolute percentage error (*MAPE*), mean absolute error (*MAE*), mean square error (*MSE*), and root mean square error (*RMSE*) values [18-22].

Results and Discussion

This section conducted a correlation analysis on the five main parameters (*T, P, F, L_b,* and L_w) affecting the energy levels of electrons in the AlGaAs quantum well structure and dipole moment matrix elements. This analysis predicts how the main and sub-parameters alter the optical and electronic properties of electrons confined in quantum wells. The changes in the energy levels of electrons within the well under the influence of external fields explain the variation in the NOR peak value. These external fields have significant effects on the NOR coefficient and play a crucial role in determining the changes that structural parameters can induce in the system's nonlinear optical properties

Table 1.(a) Correlation Analysis Values of the Temperature Main Parameter with Each Sub-Parameter.

	Correlation	*p-value*
T-E_{10}	0.9842	0.0023
T-E_{20}	0.9726	0.0054
T-E_{30}	0.9764	0.0043
T- $\mu_{01}^2\delta_{01}$	0.9572	0.0105
T- $\mu_{01}\mu_{12}\mu_{20}$	0.9690	0.0065
T- $\mu_{01}\mu_{12}\mu_{23}\mu_{30}$	0.97618	0.0043

Table 1.(b) Correlation Analysis for Photon Energy (ω (meV)) Values at Which NOR Reaches Its Maximum for Different Temperature Values.

T (K)	*ω*	*NOR*
100	7.1	25.500
300	7.4	25.648
500	7.7	26.160
700	8.2	26.629
900	8.7	27.2747
Correlation		*p-value*
0.9939		0.0005

Findings related to *RQ1:* As temperature (T) increases, a strong, positive, and statistically significant correlation is observed between the energy level differences and dipole moment matrix elements, indicating that T has a predictable effect on these parameters.

Findings related to *RQ2:* At a temperature of T = 100K, a significant negative correlation is observed between photon energy and maximum NOR values, clearly highlighting the impact of temperature on the NOR signal.

Findings related to *RQ3:* A strong positive correlation was found between temperature and photon energy, indicating that as temperature increases, the NOR maximum peak value shifts to higher energy regions (blue region).

As temperatures increase, E_{10}, E_{20}, and E_{30} follow a specific trend, while dipole moment matrix elements also increase. Table 1 (a) shows that the p-values (< 0.05) indicate statistically significant correlations between *T* and the sub-parameters. A strong positive correlation exists between *T* and the first three sub-parameters, suggesting that temperature significantly affects energy levels and dipole moments. This means energy differences and dipole moments change predictably with temperature, causing the NOR peak to shift towards the blue region. Similarly, *T* also shows a positive correlation with the last three sub-parameters, which influence NOR intensity, indicating that higher temperatures increase NOR values. Table 1 (b) the photon energy values at which the NOR reaches its maximum were examined, and a correlation analysis was conducted to understand the relationship between these values. This allowed for a detailed exploration of how the nonlinear optical response changes at different energy levels and how it interacts with external factors.

As seen in Table 2 (a), there is a strong negative correlation between E_{10}, E_{20}, E_{30}, and pressure (*P*) (r<-0.99). Positive correlations exist between the μ values and *P* ($r > 0.94$). The p-values between *P* and the sub-parameters are quite small (< 0.05), indicating that the results are statistically significant. There is an inverse relationship between *P* and the first three sub-parameters. These strong negative correlations demonstrate the significant diminishing effect of pressure on energy levels. This suggests that pressure is important in predicting the differences between energy levels. This also indicates that the NOR optical coefficient shifts in the opposite direction (towards the red region) as pressure increases. The positive correlations show that dipole moments increase with pressure. Correlation analyses can predict the behavior of energy levels and dipole moments as a function of pressure by using these relationships. As seen in Table 2 (b), as the pressure value increases, the photon energy at which the NOR coefficient reaches its maximum peak decreases. This strong correlation indicates that an increase in pressure diminishes the photon energy at which the NOR maximum peak occurs. Machine learning models can use such a relationship to predict photon energy and NOR values based on pressure. This means that with increasing pressure, the photon energy corresponding to the NOR maximum peak decreases, leading to a shift of the NOR peak towards lower energy regions (redshift).

Table 2.(a) Correlation Analysis Values of the Pressure Main Parameter with Each Sub-Parameter.

	Correlation	*p-values*
P -E_{10}	-0.9988	0.0011
P -E_{20}	-0.9997	0.0002
P -E_{30}	-0.9998	0.0001
P - $\mu_{01}^2\delta_{01}$	0.9827	0.0172
P - $\mu_{01}\mu_{12}\mu_{20}$	0.9443	0.0556
P - $\mu_{01}\mu_{12}\mu_{23}\mu_{30}$	0.9483	0.0516

Table 2.(b) Correlation Analysis for Photon Energy (ω (meV)) Values at Which NOR Reaches Its Maximum for Different Pressure Values.

P	*ω*	*NOR*
0	7.4	25.648
10	6.9	25.557
20	6.5	25.248
30	6	25.180
Correlation		*p-value*
0.9532		0.0467

Findings related to *RQ1:* A strong negative correlation was observed between pressure and the differences in energy levels, while a strong positive correlation was found between pressure and dipole moment matrix elements. This indicates that pressure has a diminishing effect on energy levels and an enhancing effect on dipole moments, causing the NOR optical coefficient to shift towards the red region as pressure increases.

Findings related to *RQ2:* In the case of P = 0 kbar, a significant negative correlation was observed between photon energy and maximum NOR values, indicating that, when pressure is zero, the NOR signal is related to the independent variables.

Findings related to *RQ3:* A strong negative correlation was found between pressure and photon energy, indicating that as pressure increases, the NOR maximum peak value shifts to lower energy regions (red shift), and the photon energy decreases.

As seen in Table 3 (a), the correlation analyses between the electric field and the sub-parameters are presented. Strong positive correlations exist between E_{10}, E_{20}, and E_{30} with the electric field (F) (p<0.05). The p-values between the electric field and sub-parameters are less than 0.05, making the analysis statistically significant. A positive correlation exists between F and the first three sub-parameters, indicating that as F increases, the NOR value is expected to shift towards the blue region. Negative correlations were found between the electric field (F) and the dipole moment matrix elements corresponding to the last three sub-parameters ($p < 0.05$). The last three parameters determine the intensity of the NOR values. These results show that energy levels rise as the electric field increases, but the value of dipole moments decreases. The increase in the electric field causes energy levels to shift towards the blue region, while the decrease in dipole moments leads to a reduction in the intensity of the NOR peak. As seen in Table 3 (b), with increasing F values, the photon energy values at which the NOR coefficient reaches its maximum peak also increase. This indicates that the NOR maximum peak value shifts to higher energy regions as the electric field increases. The correlation analysis results show a strong negative correlation between the electric field (F) and photon energy (p < 0.05), which suggests that the NOR maximum peak value shifts to higher energy regions. As the F value increases, the photon energy values corresponding to the NOR maximum peak also increase. With increasing electric field values, the NOR peak shifts to the higher energy region (blue shift).

Table 3.(a) Correlation Analysis Values of the Electric Field Main Parameter with Each Sub-Parameter.

F	ω	NOR
0	7.4	25.648
30	24.9	22.832
60	48.3	17.395
90	72.0	9.956
Correlation		*p-value*
-0.991379		0.008620

Table 3.(b) Correlation Analysis for Photon Energy (ω (meV)) Values at Which NOR Reaches Its Maximum for Different Electric Field Values.

	Correlation	*p-value*
F-E_{10}	0.9975	0.0024
F-E_{20}	0.9976	0.0023
F-E_{30}	0.9837	0.0162
F- $\mu_{01}^2\delta_{01}$	-0.8700	0.1299
F- $\mu_{01}\mu_{12}\mu_{20}$	-0.9196	0.0803
F- $\mu_{01}\mu_{12}\mu_{23}\mu_{30}$	-0.9716	0.0283

Findings related to *RQ1:* The increase in the electric field causes strong positive correlations in the energy level differences (shifting towards the blue region) and negative correlations in the dipole moment matrix elements (leading to a decrease in the NOR peak intensity).

Findings related to *RQ2:* In the case of zero electric field, a negative correlation is observed between NOR maximum values and photon energy, and this correlation is found to be significant.

Findings related to *RQ3:* With increasing electric field values, the photon energy corresponding to the NOR maximum peak shifts to higher energy regions (blue shift), and a strong positive correlation is found between this relationship.

As seen in Table 4 (a), the p-values between the barrier thickness and the sub-parameters are less than 0.05, indicating that the analyses are statistically significant. A negative correlation exists between barrier thickness (L_b) and energy levels. There is an inverse relationship between barrier thickness and the first three sub-parameters, with negative correlation coefficients and close to -1. As the barrier thickness increases, the NOR optical coefficient moves in the opposite direction, and the peak position shifts to lower energy regions. A positive correlation is found between L_b and dipole moment matrix elements. Similarly, the last three sub-parameters are positively affected by increasing L_b, which indicates an increase in peak amplitude. These correlations reveal that as barrier thickness increases, the differences between energy levels decrease, and dipole moments increase. As a result, with increasing barrier thickness, the peak positions shift to lower energies and peak amplitudes increase. In the analysis presented in Table 4 (b), the photon energy values at which NOR reaches its maximum were examined, and a correlation analysis was conducted to understand the relationship between these values. This details the changes in nonlinear optical response at different energy levels and how it interacts with the applied pressure. Table 4 shows that as barrier thickness increases, the photon energy values at which the NOR coefficient reaches its maximum peak decrease. The correlation value is -0.984, and the p-value is 0.016. These findings show that as barrier thickness (L_b) increases, the photon energy corresponding to the NOR maximum peak decreases, causing the energy to shift to lower energy regions (redshift).

Table 4.(a) Correlation Analysis Values of the Barrier Thickness Main Parameter with Each Sub-Parameter.

	Correlation	p-values
L_b-E_{10}	-0.9542	0.0457
L_b-E_{20}	-0.9466	0.0533
L_b-E_{30}	-0.9887	0.0112
L_b- $\mu_{01}^2\delta_{01}$	0.9989	0.0010
L_b-$\mu_{01}\mu_{12}\mu_{20}$	0.9700	0.0299
L_b-$\mu_{01}\mu_{12}\mu_{23}\mu_{30}$	0.9976	0.0023

Table 4.(b) Correlation Analysis for Photon Energy (ω (meV)) Values at Which NOR Reaches Its Maximum for Different Barrier Thickness Values.

L_b	ω	NOR
2	36.8	2.880
3	17.8	9.984
4	8.6	11.253
5	4.1	14.634
Correlation		p-value
-0.9843		0.0156

Findings related to *RQ1:* The increase in barrier thickness leads to a decrease in the differences between energy levels and an increase in dipole moments, causing the peak positions to shift to lower energy regions and the peak amplitude to rise.

Findings related to *RQ2:* When the quantum barrier thickness (L_b) is 3 nm, a strong negative correlation is found between L_b and the NOR maximum peak value, and this relationship is statistically significant.

Findings related to *RQ3:* As the barrier thickness increases, the photon energy corresponding to the NOR maximum peak decreases, and this energy shifts to lower energy regions (red shift). The results of the correlation analysis show that this relationship exhibits a strong negative correlation, and the p-value is statistically significant.

From Table 5 (a), it can be observed that the correlations between the parameters E_{10}, E_{20}, and E_{30} with Lcw are negative and close to -1. This indicates that as the barrier width (Lc_w) increases, the differences between energy levels decrease. The positive correlation between the dipole moment matrix elements and Lc_w suggests that these parameters increase with the rise in barrier width. The increase in barrier width reduces the energy level differences and causes the electrons to shift to lower energy regions. This shows that the optical properties of the system become more pronounced in the lower energy regions. In Table 5 (a), it is also noted that the *p*-values between Lc_w and the sub-parameters are less than 0.05, confirming that the analyses are statistically significant. A negative relationship is found between Lc_w and the first three sub-parameters, indicating that as the barrier width increases, the NOR optical coefficient moves in the opposite direction, and the peak position shifts to the lower energy region. Similarly, the increase in Lcw, increasing peak amplitude, positively affects the last three sub-parameters. Table 5 (b), the photon energy values at which the NOR value reaches its maximum are examined, and a correlation analysis has been conducted to evaluate the relationship between these values. This allows for a detailed understanding of how the nonlinear optical response at different energy levels changes and interacts with the quantum well width (Lc_w). Table 5 (b) shows that the correlation value is negative, and the *p*-value is less than 0.05. It is determined that as the Lc_w value increases, the photon energy values corresponding to the maximum NOR peak decrease. This indicates that with an increase in Lc_w, the photon energy corresponding to the NOR maximum peak decreases and shifts to the lower energy region (redshift). In other words, as Lc_w increases, the NOR peak value shifts to the lower energy regions.

Table 5.(a) Correlation analysis values of the barrier width main parameter with each sub-parameter.

c	*Correlation*	*p-values*
Lc_w -E_{10}	-0.9803	0.0196
Lc_w -E_{20}	-0.9769	0.0230
Lc_w -E_{30}	-0.9962	0.0037
Lc_w - $\mu_{01}^2\delta_{01}$	0.9997	0.0002
Lc_w - $\mu_{01}\mu_{12}\mu_{20}$	0.9989	0.0010
Lc_w - $\mu_{01}\mu_{12}\mu_{23}\mu_{30}$	0.9929	0.0070

Table 5. (b) Correlation analysis of photon energy (ω (meV)) values, at which the NOR reaches its maximum, for different barrier width values.

Lc_w	ω	*NOR*
4	11.1	17.962
5	7.4	25.648
6	5.1	35.723
7	3.4	48.199
Correlation		*p-values*
-0.960553		0.039446

Findings related to *RQ1:* As the barrier width increases, the differences between energy levels decrease, electrons shift to lower energy regions, dipole moment matrix elements and peak amplitude increase.

Findings related to *RQ2:* There is a negative correlation between the increase in quantum well width (Lc_w) and the maximum NOR values, with the maximum NOR values decreasing as the width increases.

Findings related to *RQ3:* As the well width increases, the photon energy corresponding to the NOR peak value decreases and shifts to lower energy regions (red region), and this relationship has been confirmed with a negative correlation.

Regression of NOR Peak in Quantum Wells with Selected Parameters

In this section, a regression analysis has been conducted on the effects of external fields applied to the quantum well structure on the energy levels of electrons. The regression analysis aims to predict the impact of these parameters on the optical and electronic properties of electrons confined in quantum wells and to understand how these effects are reflected in nonlinear optical responses.

In the experiments, the modeling process was carried out using a cross-validation framework to ensure robust performance evaluation and to minimize the risk of overfitting. Specifically, a 5-fold cross-validation strategy was adopted. In this approach, the dataset is randomly

partitioned into five equal subsets. At each iteration, four subsets are used for training the model, while the remaining subset is reserved for validation. This procedure is repeated five times so that each subset serves once as the validation set. The final performance metrics are then obtained by averaging the results across all folds, which provides a more reliable and generalizable estimate of the model's predictive capability compared to a single train–test split.

The graphs shown in Figure 2 compare the performance of three different models (linear, quadratic, and cubic) and explain their performance across various metrics. These performance metrics include statistical parameters such as R^2, MAPE, MAE, MSE, and RMSE, while the final graph analyzes the NOR value.

In Figure 2(a), the R^2 value is examined. The cubic model has the highest R^2 value, meaning it provides a better fit compared to the other two models. The quadratic and linear models have lower R^2 values, but the quadratic model performs slightly better than the linear model. Figure 2 (b) presents MAPE, which measures the percentage error of a model. The cubic model has the lowest MAPE value, indicating that it produces the most accurate predictions. The other two models have significantly higher MAPE values, suggesting their predictions are less accurate. In Figure 2 (c), MAE measures the average magnitude of prediction errors in the model. The cubic model has the lowest MAE value, meaning its prediction errors are much smaller than those of the other models. The quadratic and linear models have higher MAE values, but the quadratic model again performs better than the linear model. MSE, which measures the average squared difference between observed and predicted values, is presented in Figure 2 (d). Lower MSE values indicate that predictions are closer to observed values. The cubic model has the lowest MSE, while the linear and quadratic models have higher values, suggesting larger prediction errors in those models. RMSE, the square root of MSE, measures the standard deviation of prediction errors. As shown in Figure 2 (e), the cubic model has the lowest RMSE value, demonstrating the highest prediction accuracy. The quadratic and linear models have higher RMSE values, but the quadratic model again outperforms the linear model. Figure 2 (f) compares the NOR values for the three models. The NOR peak value is analyzed as a function of photon energy. The cubic model captures the NOR peak value more accurately, while the linear and quadratic models exhibit deviations from the true NOR behavior. This graph clearly shows that the cubic model best fits the data.

The cubic model provided a better R^2 value (R^2 = 0.804) for the temperature parameter in the regression analyses. The analysis of the model was found to be significant. The cubic model equation and constants defining the NOR coefficient for the temperature parameter are given in Equation 4.

$$NOR = 2.97x_0 - 0.305x_0^2 + 0.007x_0^3 + c \quad (4)$$

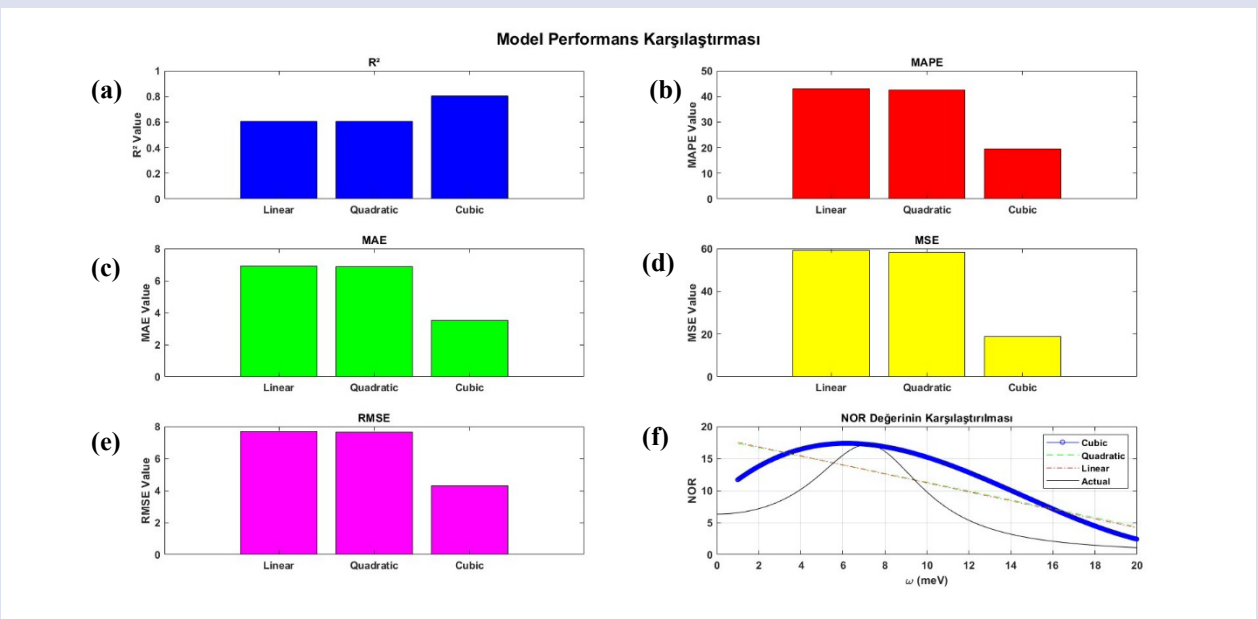

Figure 2. Evaluation metrics for temperature and comparison of NOR value across three models.

The graphs in Figure 3 provide a detailed comparison of the performance of the linear, quadratic, and cubic models for the pressure parameter, illustrating how each model performs for specific pressure values. Figure 3 (a), the cubic model has the highest R2 value. The linear and quadratic models have lower R2 values. Figure 3 (b) compares the MAPE values of the models, showing that the cubic model has the lowest MAPE, indicating the highest prediction accuracy and lower error rates compared to the other models. Figure 3 (c) presents the MAE values, where the cubic model again has the lowest MAE, indicating smaller prediction errors and a better alignment with the observed data compared to the other models. In Figure 3 (d), the cubic model has the lowest MSE, providing the most accurate predictions closest to the observed values. Figure 3 (e) shows that the cubic model achieves the lowest RMSE, further confirming that the cubic model has the smallest prediction errors and a higher accuracy rate than the other models. Figure 3 (f) presents a comparison of the NOR values for the three

models. In modeling the NOR peak value as a function of photon energy (ω), the cubic model provides the most accurate predictions, while the linear and quadratic models exhibit significant deviations from the peak value.

The cubic model was determined to provide the best R^2 value (R^2 = 0.804) for the pressure parameter in the regression analyses. This allowed for a more accurate explanation of the relationship between the parameters and pressure. Equation 5 provides the equation defining the cubic value.

$$NOR = 3.246x_0 - 0.321x_0^2 + 0.007x_0^3 + c \quad (5)$$

Findings related to *RQ4*: The cubic model provides the best R^2 value (R^2=0.804) for the pressure parameter, allowing for more accurate explanations.

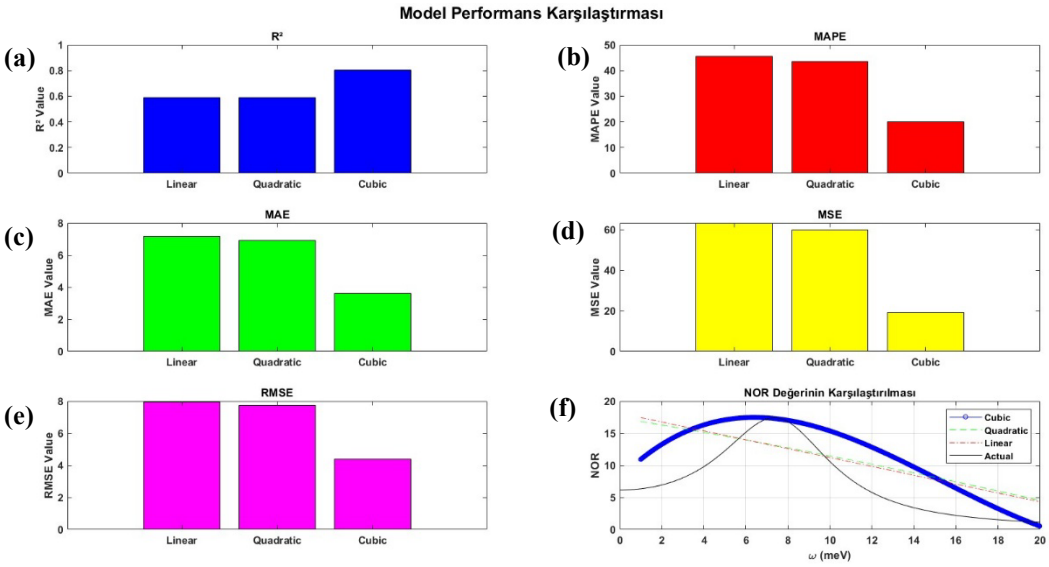

Figure 3. Comparison of evaluation metrics and NOR values for pressure across three models.

Figure 4 provides a detailed comparison of the performance of the linear, quadratic, and cubic models for the electric field parameter, analyzing how each model performs at different electric field values. This performance analysis evaluates the models' accuracy and prediction capabilities using statistical metrics such as R^2, MAPE, MAE, MSE, and RMSE. Additionally, the last graph analyzes the NOR value for different photon energies (ω). In Figure 4 (a), the R^2 values of the models are compared. The cubic model has the highest R^2 value, indicating a better fit to the data. In contrast, the quadratic model performs slightly better than the linear model but does not achieve the success of the cubic model. In Figure 4 (b), the MAPE values are used to compare the prediction accuracy of the models. The cubic model has the lowest MAPE, providing the most accurate predictions, while the linear and quadratic models have higher MAPE values, suggesting greater prediction errors. Figure 4 (c) compares the MAE values, showing that the cubic model has the lowest MAE, indicating smaller prediction errors compared to the other models. In Figure 4 (d), the MSE values are analyzed, with the cubic model providing the lowest MSE, indicating that its predictions are closer to the observed data. Figure 4 (e) compares the RMSE values, revealing that the cubic model has the lowest RMSE, meaning that its predictions are more consistent with smaller errors. Figure 4 (f) compares the NOR values for the three models. The cubic model accurately predicts the NOR peak value, achieving significantly better results than the other models. Overall, the analyses in Figure 4 show that the cubic model outperforms the linear and quadratic models across all performance metrics and provides the best results, particularly in predicting the NOR peak value.

As a result of the regression analyses, the cubic model provides a higher R^2 value for the electric field parameter. Therefore, the cubic model was preferred in the regression analyses. The R^2 value was determined to be 0.805, indicating that the model successfully explains the data. For the variation in electric field values, the equation explaining the NOR behavior was obtained using the cubic model, as shown below. This equation reveals that the NOR value exhibits linear, quadratic, and cubic relationships with the electric field, as shown in Equation 6.

$$NOR = 3.283x_0 - 0.325x_0^2 + 0.007x_0^3 + c \quad (6)$$

Findings related to *RQ4:* The variation in the electric field affects the NOR value, and the cubic model provides the most accurate explanation of the relationship between the electric field and the NOR coefficient, delivering the best performance compared to the other models.

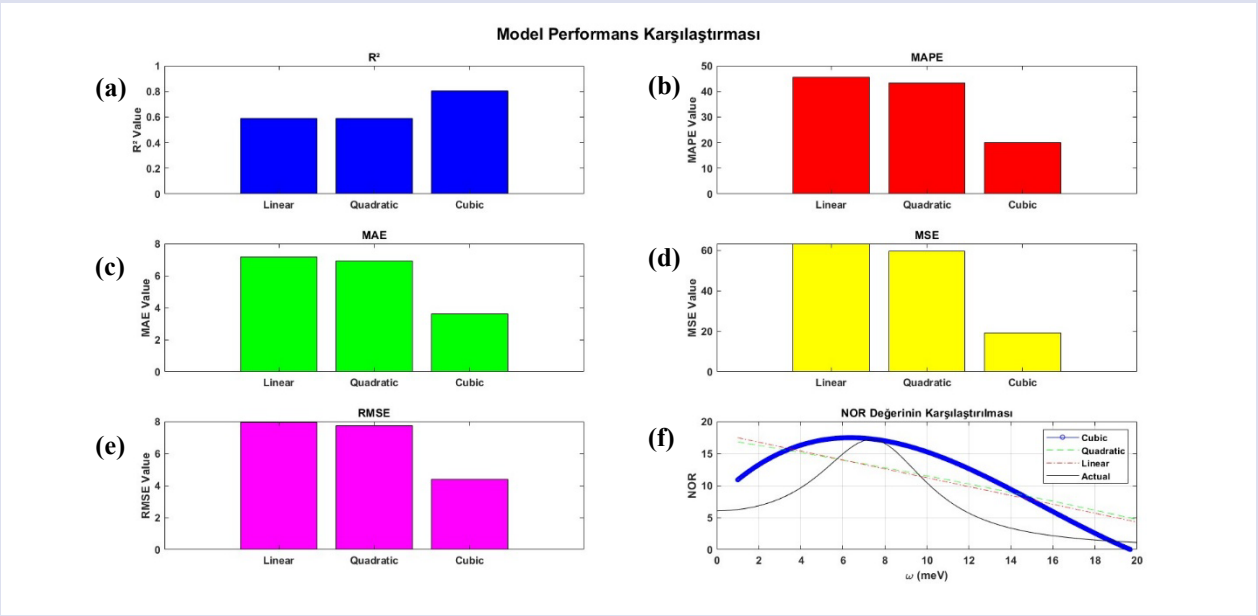

Figure 4. Comparison of evaluation metrics and NOR values for the electric field value across three models.

In Figure 5 (a), the R^2 values of the linear, quadratic, and cubic models are compared. Figure 5 (b) compares the MAPE values. The cubic model achieves the lowest MAPE value, providing the most accurate predictions. While the quadratic model gives better results than the linear model, it still does not reach the performance of the cubic model. Figure 5 (c) compares the MAE values, showing that the cubic model has the lowest MAE value, offering more accurate predictions than the other models. Figure 5 (d) compares the MSE values, with the cubic model providing the lowest MSE, indicating that it makes accurate predictions and is closer to the observed data. Figure 5 (e) compares the RMSE values, where the cubic model, with the lowest RMSE value, is sensitive to error magnitudes and provides the most accurate predictions. Figure 5 (f) compares the NOR values as a function of photon energy (ω). The cubic model, shown by the blue curve, best reflects the actual NOR behavior, particularly producing accurate results at high photon energy values. While the quadratic model performs better than the linear model, it fails to capture the NOR peak value accurately. The linear model shows deviations from the NOR peak points, indicating that it does not sufficiently explain the NOR behavior.

The cubic model provides the highest R^2 value for barrier thickness in the regression analyses. The analysis using the cubic model yielded an R^2 value of 0.649, indicating that this model provides the best R^2 value.

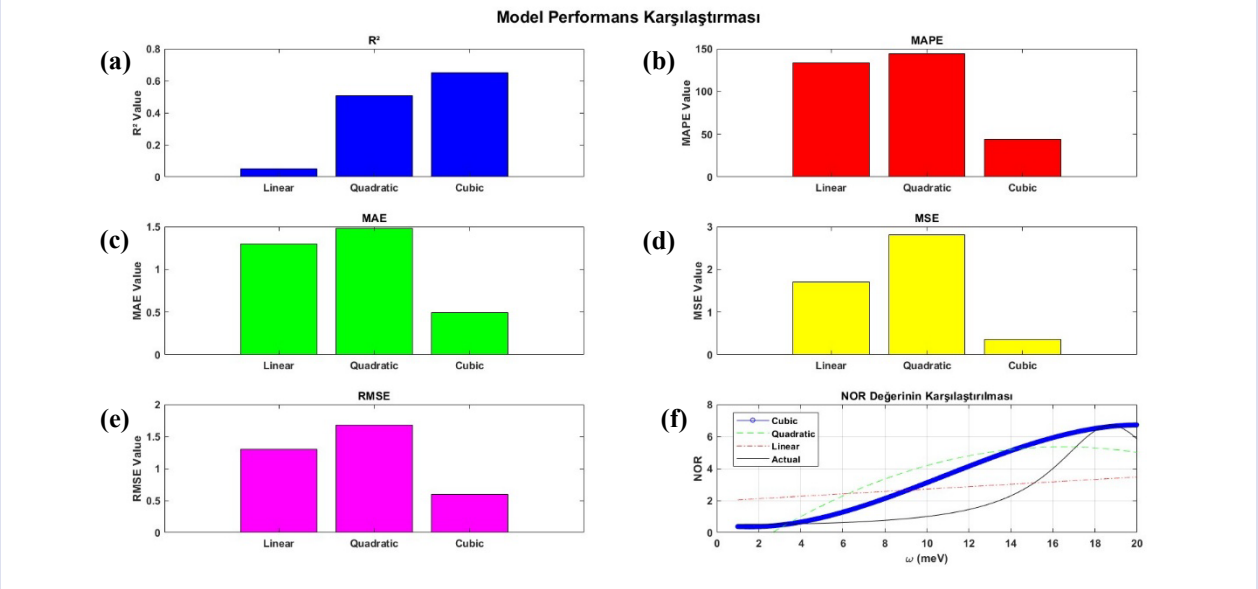

Figure 5. Comparison of evaluation metrics and NOR values for the barrier thickness across three models.

The cubic model offers a significant and good fit in the regression analyses. The resulting regression equation is given in Equation 7.

$$NOR = -0.189x_0 - 0.065x_0^2 + 0.002x_0^3 + c \quad (7)$$

Findings related to *RQ4:* The cubic model was used to explain the relationship between the barrier thickness parameter and the NOR coefficient, and it was observed that this model provided the best fit with an R^2 value of 0.649.

Figure 6 (a) shows that the quadratic model best fits the data and explains the changes in the NOR peak more accurately than the other models. While performing better than the linear model, the cubic model does not match the quadratic model's success when considering the evaluation metrics. In Figure 6 (b), the quadratic model achieves the lowest MAPE value, making the most accurate predictions. Figure 6 (c) demonstrates that the quadratic model also has the lowest MAE value, providing the most accurate NOR predictions. In Figure 6 (d), the quadratic model, with the lowest MSE value, shows that its predictions are closest to the observed data. In Figure 6 (e), the quadratic model, with the lowest RMSE value, exhibits the smallest prediction errors. Figure 6 (f) shows how the NOR values change with photon energy, and the quadratic model provides the best fit for photon energy, capturing the NOR peak more accurately. While the cubic model performs slightly lower, it still fits better than the linear model.

The cubic model provides a higher R^2 value for barrier width in the regression analyses conducted. Therefore, the cubic model was preferred in the regression analyses. The cubic model was selected as the best model, and the R^2 value was found to be 0.725. The quadratic regression equation obtained for the cubic model is given

$$NOR = 0.929x_0 - 0.040x_0^2 + 0x_0^3 + c \quad (8)$$

Findings related to *RQ4:* The cubic model provides a higher R^2 value for quantum well width, but the quadratic model, with lower evaluation metrics, demonstrates more efficient performance and therefore predicts the NOR values more accurately.

The optical response of a quantum well is strongly influenced by several external and structural parameters, including temperature, applied electric field, pressure, and the geometric characteristics of the well. Temperature changes affect the band structure through band-gap narrowing and enhanced carrier–phonon scattering. Applied electric fields modify the confinement potential via the quantum-confined Stark effect, causing shifts in energy levels and corresponding changes in nonlinear optical responses. Pressure variations alter the lattice constant and induce strain, shifting band edges and transition energies, while changes in geometric characteristics influence confinement energies and wavefunction overlap, directly impacting sub-band levels and transition strengths. Together, these factors determine the quantum well's optical behavior under varying conditions.

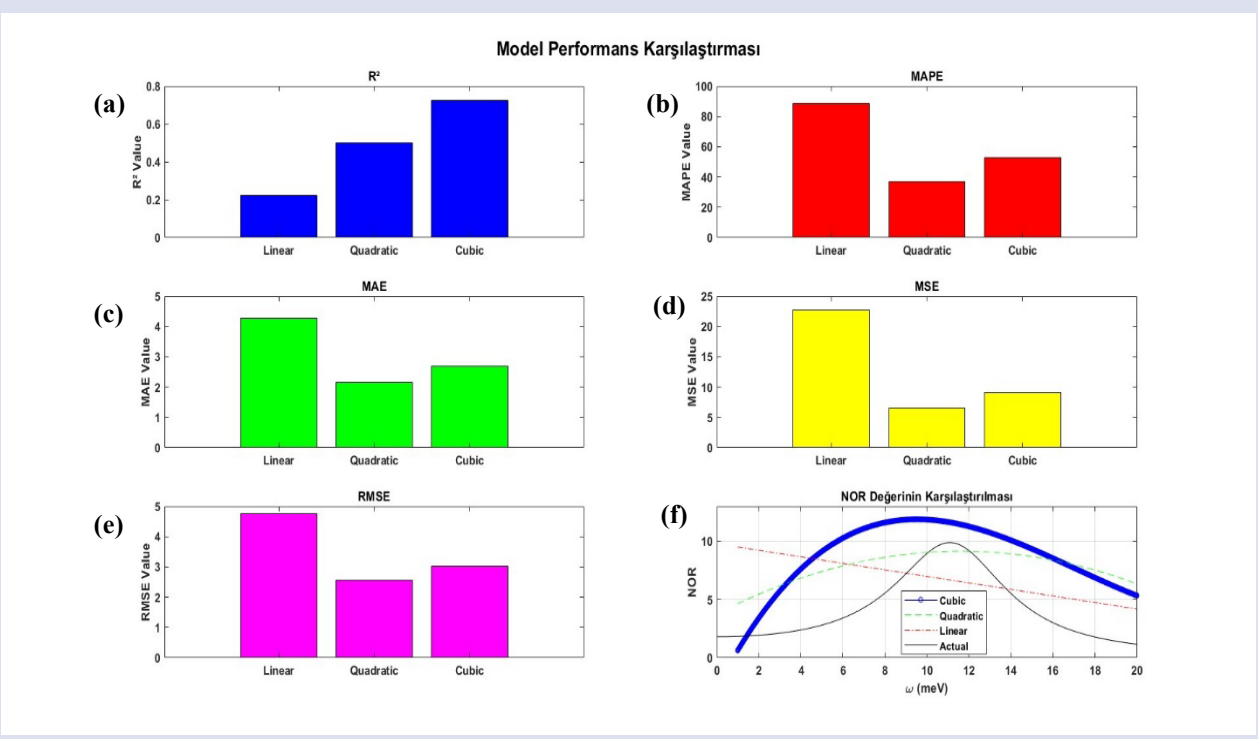

Figure 6. Comparison of evaluation metrics and NOR values for the barrier width value across three models.

Conclusion and Future Work

The widespread use of semiconductor technologies has led to increased research on high-tech products. The study of the electronic and optical properties of quantum well-based systems provides numerous advantages in terms of product optimization.

After the energy eigenvalues and eigenfunctions of the confined electrons in the QW structure were determined, the NOR coefficient of the system was calculated numerically. In this context, the NOR coefficient behavior of the material system was investigated under the influence of different structural parameters and external fields using regression and correlation analyses. In QW design, parameters such as barrier width, barrier thickness, and applied external fields (temperature, pressure, and electric field) were controlled, the difference between the electron's ground and excited energy levels was observed, and dipole moment values were obtained.

QW design was performed using Matlab software, and the system's energy values and eigenfunctions were numerically calculated under various structural parameters and external fields. Regression and correlation analyses of the obtained energy eigenvalues and matrix elements were performed using the IBM SPSS Statistics program. The accuracy and effectiveness of the model were evaluated using linear, quadratic, and cubic regression analyses. As a result, it was determined that the cubic regression model provided the best fit for the system. Evaluation metrics obtained from the regression analysis, such as R^2, MAPE, MAE, MSE, and RMSE values, were calculated.

For each external parameter (T, P, F, L_b, L_w), evaluation metrics and NOR values defining three models were compared, and it was generally found that the cubic model gave the best results. In this study, the QW structure was designed, and the system's NOR coefficient behavior was modeled through correlation and regression analyses before experimental work. This approach enabled experimental studies to be carried out more economically and efficiently in time.

In future studies, the predictive modeling approach applied in this research can be further enhanced by integrating advanced machine learning algorithms, such as neural networks and ensemble learning, to improve the accuracy of NOR predictions in quantum wells. Additionally, incorporating experimental validation of the regression-based models will strengthen their reliability and applicability in real-world optoelectronic device design. Expanding the study to include other nonlinear optical phenomena, such as second and third harmonic generation, could provide a more comprehensive understanding of quantum well structures under varying external conditions. Moreover, exploring the effects of different semiconductor materials and quantum well geometries on NOR behavior may offer new insights into optimizing optical responses for next-generation photonic applications.

Conflicts of interest

The authors state that they do not have a conflict of interest.

Acknowledgment

This study is part of Muhammed Sayrac's master's thesis in the Department of Artificial Intelligence and Data Science, under the Computer Engineering Department at Sivas Cumhuriyet University.

References

[1] Heinen B., Wang T. L., Sparenberg M., Weber A., Kunert B., Hader J., and Stolz W., Pushing the output powers of transversal multimode VECSELs beyond the 100 W barrier. in ISLC 2012 *International Semiconductor Laser Conference*. 2012.

[2] Karim A., Bjorlin S., Piprek J., and Bowers J. E., Long-wavelength vertical-cavity lasers and amplifiers. *IEEE Journal of Selected Topics in Quantum Electronics*, 6 (2000) 1244-1253.

[3] Alford W.J., T.D. Raymond, and A.A. Allerman, High power and good beam quality at 980 nm from a vertical external-cavity surface-emitting laser. *Journal of the Optical Society of America B*, 19 (2002) 663-666.

[4] Sayraç H., Sayraç M., and Elagöz S., GaAs Alttaş Üzerine Büyütülen GaAs/GaAlAs Heteroyapılarının Yüksek Çözünürlüklü X- Işını Kırınım Yöntemi Kullanılarak Karakterizasyonu. *Afyon Kocatepe Üniversitesi Fen Ve Mühendislik Bilimleri Dergisi*, 20 (2020) 558-564.

[5] Liang B.W. and C.W. Tu, A kinetic model for As and P incorporation behaviors in GaAsP grown by gas-source molecular beam epitaxy. J*ournal of Applied Physics*, 74 (1993) 255-259.

[6] Tuzemen A. T., Al E. B., Sayrac H., Dakhlaoui H., Mora-Ramos M. E., and Ungan F. Effects of hydrostatic pressure, temperature, and position-dependent mass on the nonlinear optical properties of triple delta-doped GaAs quantum well. *The European Physical Journal Plus*, 139 (2024) 690.

[7] Dakhlaoui H., J.A. Vinasco, and C.A. Duque, External fields controlling the nonlinear optical properties of quantum cascade laser based on staircase-like quantum wells. *Superlattices and Microstructures*, 155 (2021) 106885.

[8] Sayrac H., Dakhlaoui H., Mora-Ramos M. E., and Ungan F., Influence of external probes on the nonlinear optical characteristics of a GaAs/AlGaAs quantum well with an anharmonic potential. *Optical and Quantum Electronics*, 57 (2025) 43.

[9] Pal S. and M. Ghosh, Tailoring nonlinear optical rectification coefficient of impurity doped quantum dots by invoking Gaussian white noise. *Optical and Quantum Electronics*, 48 (2016) 372.

[10] Sayrac H., Jaouane M., Ed-Dahmouny A., Sali A., and Ungan F., Modulation of nonlinear optical rectification, second, and third harmonic generation coefficients in n-type quadruple δ-doped GaAs quantum wells under external fields. *Physica B: Condensed Matter*, 690 (2024) 416252.

[11] Khordad R., Effects of magnetic field and geometrical size on the interband light absorption in a quantum pseudodot system. *Solid State Sciences*, 12 (2010) 1253-1256.

[12] Hien N.D., Linear and nonlinear optical properties in quantum wells. *Micro and Nanostructures*, 170 (2022) 207372.
[13] Feddi E., Assaid E., Dujardin F., Stébé B., and Diouri J., Magnetic Field Influence on the Polarisability of Donors in Quantum Crystallites. *Physica Scripta*, 62 (2000) 88.
[14] Dakhlaoui H. and M. Nefzi, Tuning the linear and nonlinear optical properties in double and triple δ− doped GaAs semiconductor: Impact of electric and magnetic fields. *Superlattices and Microstructures*, 136 (2019) 106292.
[15] El-Mahalawy A.M. and K.H. El-Safty, Classical and quantum regression analysis for the optoelectronic performance of NTCDA/p-Si UV photodiode. *Optik*, 246 (2021) 167793.
[16] Mishima T.D. and M.B. Santos, Regression Analysis for Transport Electron Scattering Caused by Structural Defects in InSb Quantum Wells: Application of Matthiessen's Formula. Japanese *Journal of Applied Physics*, 51 (2012) 06FE07.
[17] Eseanu N., Simultaneous effects of laser field and hydrostatic pressure on the intersubband transitions in square and parabolic quantum wells. *Physics Letters A*, 374 (2010) 1278-1285.
[18] Dursun Ö.O. and S. Toraman, Uzun Kısa Vadeli Bellek Yöntemi ile Havayolu Yolcu Tahmini. *Journal of Aviation*, 5 (2021) 241-248.
[19] Yerel S. and T. Ersen, Prediction of the Calorific Value of Coal Deposit Using Linear Regression Analysis. *Energy Sources, Part A: Recovery, Utilization, and Environmental Effects*, 35 2013 976-980.
[20] Çıtakoğlu H. and Ö. Coşkun, Dalgacık Dönüşüm Modelli Yapay Zekâ Teknikleri Kullanılarak Orta Anadolu Bölge İstasyonlarının Yağış Tahmini. *Harran Üniversitesi Mühendislik Dergisi*, 6 2021 39-54.
[21] Chai T. and R.R. Draxler, Root mean square error (RMSE) or mean absolute error (MAE)? – Arguments against avoiding RMSE in the literature. *Geosci. Model Dev.*, 7 (2014) 1247-1250.
[22] Hodson T.O., Root-mean-square error (RMSE) or mean absolute error (MAE): when to use them or not. *Geosci. Model Dev.*, 15 (2022) 5481-5487.